JGR Oceans

RESEARCH ARTICLE
10.1029/2020JC017075

Revisiting the Recharge and Discharge Processes for Different Flavors of El Niño

Soumi Chakravorty[1], Renellys C. Perez[2], C. Gnanaseelan[3], and Bruce T. Anderson[4]

[1]Cooperative Institute for Marine and Atmospheric Studies, University of Miami, Miami, FL, USA, [2]NOAA Atlantic Oceanographic and Meteorological Laboratory, Miami, FL, USA, [3]Indian Institute of Tropical Meteorology, Ministry of Earth Sciences, Pune, India, [4]Department of Earth and Environment, Boston University, Boston, MA, USA

Key Points:

- The Simple Ocean Data Assimilation system is used to study the composite behavior of eastern- and central-Pacific El Niño events
- Tropical Pacific subsurface recharge-discharge processes are significantly different for cold eastern- and central-Pacific El Niño events
- Positive subsurface heat content anomalies are a not a precursor of central Pacific El Niño events, making them far less predictable

Correspondence to:
S. Chakravorty,
soumi.chakravorty@noaa.gov;
soumi.chakravortyhb@gmail.com

Citation:
Chakravorty, S., Perez, R. C., Gnanaseelan, C., & Anderson, B. T. (2021). Revisiting the recharge and discharge processes for different flavors of El Niño. *Journal of Geophysical Research: Oceans*, *126*, e2020JC017075. https://doi.org/10.1029/2020JC017075

Received 14 DEC 2020
Accepted 16 OCT 2021

Author Contributions:
Formal analysis: Soumi Chakravorty
Funding acquisition: Renellys C. Perez, C. Gnanaseelan
Validation: Renellys C. Perez, C. Gnanaseelan, Bruce T. Anderson
Writing – original draft: Soumi Chakravorty
Writing – review & editing: Soumi Chakravorty, Renellys C. Perez, C. Gnanaseelan, Bruce T. Anderson

Abstract El Niño-related sea surface temperature (SST) anomalies over the tropical Pacific Ocean impact global climates, but these impacts differ substantially for conventional cold tongue El Niño (CT El Niño) and the central Pacific El Niño (CP El Niño) events. This study is motivated by the need for a better understanding of the recharge/discharge processes associated with these two different flavors of El Niño. Composite analysis based on improved CT and CP El Niño identification methods applied to the Simple Ocean Data Assimilation demonstrates that the recharge/discharge processes are active during CT El Niño events. In contrast, for CP El Niño events, the recharge/discharge processes do not play a significant role. Prior to a CT El Niño, warm water accumulates over the western Pacific due to off-equatorial anticyclonic wind stress curl. The onset of a CT El Niño is closely associated with the formation of a cyclonic atmospheric circulation over the northwest Pacific in the winter and spring, which induces westerly wind anomalies in the equatorial western Pacific and initiates eastward warm water transport. This leads to peak warming in the eastern equatorial Pacific the following winter, followed by the poleward discharge of warm water. This quasi-cyclical behavior provides a measure of predictability. In contrast, the CP El Niño events do not show a precursor subsurface warming signal along the tropical Pacific thermocline. Instead, modest warm SST anomalies appear in boreal summer and peak in the fall, with weak subsurface warming mainly in the fall during CP El Niños. Hence, CP El Niños are less predictable in terms of an equatorial thermocline precursor than CT El Niño events.

Plain Language Summary The El Niño-Southern Oscillation (ENSO) is the largest source of year-to-year climate variability. ENSO has a pronounced influence on regional and global circulation and precipitation patterns and thus has considerable worldwide socio-economical impacts. El Niño, the warm phase of ENSO, exhibits modulation in the longitudinal location of its maximum warming, creating what is referred to as ENSO diversity. For conventional El Niño events, maximum surface warming is located in the eastern equatorial Pacific, for which subsurface warming along the tropical Pacific has proven to serve as a predictor several months in advance. Previous studies disagree on whether this subsurface warming is similarly essential for El Niño events that have peak surface warming in the central Pacific. We developed an improved method for identifying these two types of El Niño in an ocean reanalysis product. Using this improved method, we find no clear evidence of a subsurface warming precursor for the central Pacific El Niño events along the equator. This lack of a tropical subsurface precursor limits our ability to predict these types of El Niño events.

1. Introduction

The El Niño-Southern Oscillation (ENSO) is the most energetic air-sea coupled process on interannual time scales and profoundly impacts the global climate. ENSO is characterized by an irregular (2–7 years) oscillation of warm and cold sea surface temperature (SST) anomalies over the eastern and central equatorial Pacific. During the ENSO warm phase (El Niño), the tropical Pacific Ocean (TPO) and overlying atmosphere couple through the Bjerknes feedback mechanism (Bjerknes, 1969). The weakening of the zonal (i.e., east-west) SST gradient over the equatorial Pacific weakens the tropical easterly trade winds, further weakening the zonal SST gradient. However, this positive feedback cannot describe the turnabout of El Nino and its transition to the La Niña (ENSO cold phase). To explain the dynamics of the ENSO cycle, Wyrtki (1975, 1985) developed the "buildup and draining" hypothesis. According to this hypothesis, the excessively strong easterly trade winds build up warm water in the western equatorial

Pacific. During an El Niño, this warm water discharges eastward and then poleward along the American coast to the subtropics, thereby terminating the El Niño. The next El Niño event cannot occur until another "buildup" of warm water occurs, but there is no required connection between successive El Niño events.

Jin (1997) extended this "buildup and draining" hypothesis and proposed a conceptual self-sustained recharge oscillator model. According to Jin (1997), the non-equilibrium between the zonally averaged thermocline depth and meridional volume transport (due to wind stress forcing) over the TPO serves as the memory of the coupled system. Prior to an El Niño, equatorial easterly winds generate two off-equatorial anticyclones, driving the equatorward water transport (convergence) and recharging the TPO with warm water. During an El Niño, westerly wind anomalies and the associated cyclonic wind stress curl discharge this warm water poleward (divergence) and lead to a shallower than normal zonal-mean thermocline (Meinen & McPhaden 2000, 2001). In addition to this meridional advective feedback, the eastward advection of positive (negative) subsurface heat content is recognized as an important process for the development of El Niño (La Niña) events (Jin & An, 1999; Picaut et al., 1997).

It is well known now that different flavors of ENSO exist in the tropical Pacific (e.g., Capotondi et al., 2015; Kug et al., 2009; Wang & Weisberg, 2000). One expression of this ENSO diversity is the longitudinal variation in the central location of SST warming. During the canonical or cold tongue (CT) El Niño events, the SST warming first appears in the eastern equatorial Pacific and extends westward. But some years, warm SST anomalies develop over the central equatorial Pacific (Capotondi et al., 2015; Timmermann et al., 2018; Wang, 1995), unlike the traditional El Niño. This second flavor of El Niño has been given various names in the literature, including the "'El Niño Modoki" (Ashok et al., 2007), warm pool El Niño (Kug et al., 2009), with central Pacific (CP) El Niño (Yeh et al., 2009) being the most commonly used. While some literature considers ENSO positioning as a continuum of events (Cai et al., 2014; Capotondi et al., 2015; Fedorov et al., 2015; Johnson, 2013; Xie & Jin, 2018; Takahashi et al., 2011), others argue that multiple ENSO flavors exist (e.g., Johnson, 2013; Lee et al., 2014, 2018; Newman et al., 2011) and that two distinct flavors are most prominent: CT and CP El Niños (Ashok et al., 2007; Capotondi et al., 2015; Ham & Kug, 2012; Kao & Yu, 2009; Ren & Jin, 2011).

Importantly, atmospheric teleconnections are distinct for different flavors of El Niño events (Karnauskas, 2013) due to their distinct spatial footprints related to the longitudinal position of SST warming and diabatic heating. The Intertropical Convergence Zone typically migrates equatorward from its mean position during CT El Niños but not during CP El Niños (Hu & Fedorov, 2018). Precipitation patterns across the globe exhibit differing relationships with the CT and CP El Niños (Feng et al., 2010; Karori et al., 2013; Lee et al., 2018; Wen et al., 2020; Xu et al., 2013, 2019). For example, CP El Niños have a more significant influence on East Asian summer monsoons during the developing phase, while CT El Niños exert a more substantial impact on Asian summer monsoons during the decaying phase (Yuan & Yang, 2012). Although CP El Niños are typically weaker than CT El Niño events (Capotondi et al., 2015), interest in CP El Niño events has also been fueled by the fact that they have become more frequent in occurrence during the late 20th century and early 21st century compared to the early 20th century (Freund et al., 2019; Lee & McPhaden, 2010; McPhaden et al., 2012; Yeh et al., 2009).

There is no consensus yet about whether the recharge-discharge (Jin, 1997) process is active during both types of El Niños, nor whether an equatorial heat content precursor exists for both types of El Niño. Some studies documented significant similarities (Feng et al., 2018; Ren & Jin, 2013; Singh & Delcroix, 2013) in the subsurface variations between these two types of El Niño events and claimed that tropical Pacific thermocline variations could be a precursor of both types of El Niño (Wen et al., 2014). Others have uncovered differences (Capotondi et al., 2015; Kug et al., 2009; Yuan & Yang, 2012) in the equatorial thermocline feedback of these two El Niño flavors. Specifically, Kug et al. (2009) found that tropical Pacific thermocline feedbacks play a significant role in the evolution of CT El Niño events. In contrast, the zonal advection of the mean SST by zonal current anomalies plays a vital role in CP El Niño events.

These seemingly conflicting findings may simply be an artifact of how CT and CP El Niño events have been defined in previous studies and may also be sensitive to which methods are used for analysis. For example, Kug et al. (2009) determined El Niño types using the Niño3 (SST anomalies averaged over 5°N–5°S,

150°W–90°W) and Niño4 (SST anomalies averaged over 5°N–5°S, 160°E–150°W) SST indices, which are highly correlated and may not be suitable for identifying diverse ENSO patterns. In contrast, Ren and Jin (2013) developed two new indices N_{CT} and N_{CP} to separate El Niño events into the two primary types and examined their evolution through regression analysis. However, we find here that the regression methods used in Ren and Jin (2013) for the N_{CT} and N_{CP} indices do not robustly separate the CT and CP El Niño events (see Section 2.2). In comparison, Singh and Delcroix (2013) used cluster analysis of sea level anomalies to isolate specific events and claimed that significant positive equatorial heat content anomalies are associated with both CP and CT El Niños. However, using sea level anomalies instead of SST anomalies in their cluster analysis may only represent the different modes of sea level variability and does not isolate the variability associated with the two El Niño types. As a result, this cluster analysis approach can lead to some sea level anomaly patterns commonly associated with the different phases of CT El Niño events to be misidentified as CP El Niño events. Thus, this type of partitioning may unduly influence composite results (e.g., Tan & Zhou, 2018).

Given these seemingly contradictory results, we will revisit the partitioning of the two types of El Niños with more care, focus on how the events are preconditioned, and examine the temporal evolution of the recharge–discharge processes associated with each event. Here, we primarily use the output from the Simple Ocean Data Assimilation (SODA; Carton & Giese, 2008) to examine the seasonal evolution of subsurface processes from the previous winter to the mature phase for both El Niño flavors. Section 2 describes the SODA reanalysis and ancillary datasets used in this analysis and the methodology to identify the two types of El Niños and construct the composites. Similarities and differences between CT and CP El Niño composites are discussed in Section 3.1. An analysis of ENSO phase diagrams and the spatial structure of the center of heat indices (CHIs) are also presented in Sections 3.2 and 3.3, respectively, to better highlight differences in the development of CT and CP El Niño events in SODA. A discussion of the EOF modes of TPO subsurface variability is provided in Section 3.4. In Section 3.5, we examine the zonal and meridional volume transports for both types of El Niño events with an eye toward how they influence the temporal evolution of those events. Lastly, we summarize the results in Section 4.

2. Data Sets and Methodology

2.1. SODA

The analysis shown in this paper mainly uses SODA (Carton & Giese, 2008) version 2.1.6, available from 1958 to 2008. For this version of SODA, the Parallel Ocean Program (Smith et al., 1992) model is forced with atmospheric data from the European Center for Medium-Range Weather Forecasts (ECMWF) Re-Analysis (ERA-40; Uppala et al., 2005) from January 1958 to December 2001 and then by QuikSCAT wind stress data for the remainder of the simulation (Risien & Chelton, 2008). To verify whether our results are robust and appear in longer SODA simulations, we repeat the analysis on SODA version 2.2.4 for 1901–2008, which uses 20CRv2c wind (Compo et al., 2011). Note, we excluded the first 40 years (1871–1900) of the SODA 2.2.4 output as the observations assimilated during that time period are very sparse (Giese & Ray, 2011).

The ENSO variability and frequency in SODA 2.1.6 and SODA 2.2.4 simulations are consistent with observations (Chakravorty et al., 2014; Giese & Ray, 2011). Specifically, SODA temperatures compare very well with expendable bathythermograph (XBT) observations. Further, these simulations have realistic representations of ENSO diversity (Chattopadhyay et al., 2019; Ray & Giese, 2012).

2.2. Identifying CT and CP El Niño Events

To focus on interannual variability, we first remove the seasonal climatology and linear trend and apply a three-month running mean low-pass filter to all SODA time-series data. Next, we modify the methodology of Ren and Jin (2013) to get a more precise separation between CT and CP El Niño events. Following Ren and Jin (2011), we calculated N_{CT} and N_{CP} indices by performing a simple weighted combination of the area-averaged Niño3 (N_3, 5°N–5°S, 150°W–90°W) and Niño4 (N_4, 5°N–5°S, 160°E–150°W) SST anomaly using the following two Equations 1 and 2.

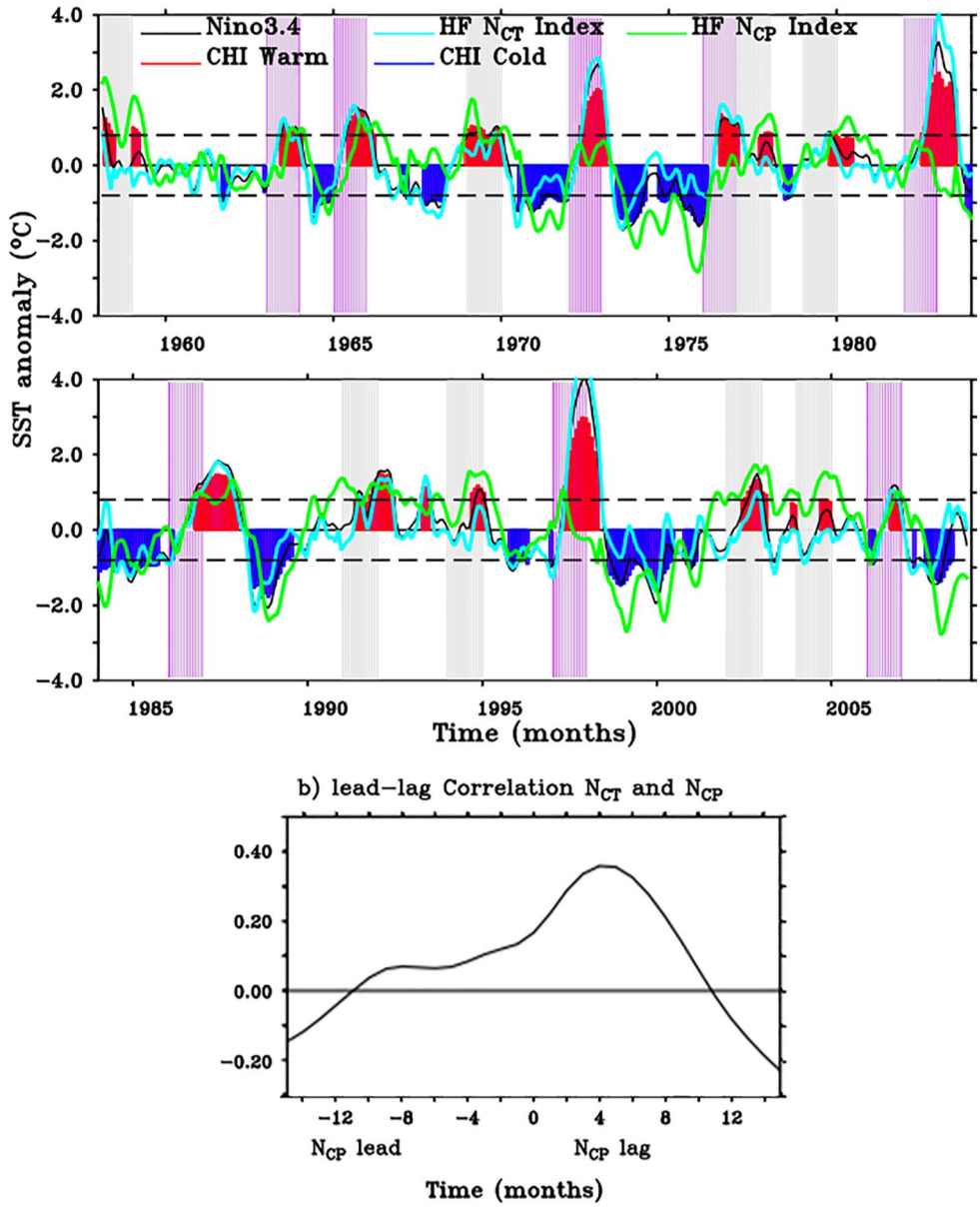

Figure 1. Simple ocean data assimilation (SODA) (a) Niño3.4 SST anomalies (black line), high-frequency (HF) HF-N_{CT} (cyan line), HF-N_{CP} (green line), center of heat index (CHI) warm (red shading), and CHI cold (blue shading) indices (see Section 2.2). The pink and gray vertical bars, respectively, denote the selected Cold Tongue (CT) El Niño and Central Pacific (CP) El Niño years. (b) 15-month lead-lag correlation between HF-N_{CT} and HF-N_{CP} indices.

$$N_{CT} = N_3 - \alpha N_4, \tag{1}$$

$$N_{CP} = N_4 - \alpha N_3 \tag{2}$$

when $N_3 \times N_4 > 0$ then $\alpha = 2/5$, else $\alpha = 0$

α is the parameter of this transformation (Ren & Jin, 2013). Then, to extract only interannual (high-frequency) variability, we high-pass filtered (HF) the N_{CT} and N_{CP} time series using a 6-year and 8-year cutoff, respectively. Figure 1a shows a time series of HF-N_{CT} and HF-N_{CP} indices (cyan and green lines, respectively) calculated from SODA 2.1.6. Ren and Jin (2011) claim that these indices separate the CT El Niño and CP El Niño events clearly. Although the simultaneous (zero-lag) correlation (Figure 1b) between the two indices is indeed low

($r \sim 0.16$), we found that the indices are significantly correlated at non-zero lags (Figure 1b), confirming that these indices are not entirely independent of one another in SODA. Although not shown, we find similar lagged co-variability between these indices when computed from the historical observed SST data from the Hadley Centre (HadISST, provided by the Met Office Hadley Centre), suggesting that lead-lag regression/correlation analysis using these two indices is not well suited to isolate the time evolution of distinct CT and CP El Niños.

We compare N_{CT} and N_{CP} indices with the surface center of heat index (CHI, red and blue shading in Figure 1), which allows the longitudinal center of SST anomalies to vary as a function of time and hence is not geographically fixed (Giese & Ray, 2011; Ray & Giese, 2012). Surface CHI is defined as the first moment of the equatorial Pacific SST anomalies (integrated between 5°S and 5°N and 120°E–80°W). If the area over which SST anomalies exceed 0.5°C is greater than or equal to the area of the Niño3.4 box for five consecutive months, then the warming event qualifies as an El Niño event. We find that not all positive HF-N_{CP} and HF-N_{CT} values are associated with significant warming (positive CHI, red shading in Figure 1a) in the equatorial Pacific and hence would have been improperly identified as warm events (e.g., 1990, 2001 would have registered as warm events using HF-N_{CP} but not using CHI). Thus, for our study, we identify the CT El Niño years as the years where HF-N_{CT} and CHI warm indices are above 0.8°C for at least five months. CP Niño events are similarly chosen as the years where HF-N_{CP} and CHI warm indices are above 0.8°C at least five consecutive months and are not already characterized as CT El Niño years. Note, with these added constraints, CP and CT events can be uniquely and objectively identified.

With this methodology, we find that in SODA 2.1.6, there are eight CT El Niño years: 1963, 1965, 1972, 1976, 1982, 1986, 1997, 2006 (pink shades in Figure 1a) and eight CP El Niño years: 1958, 1969, 1977, 1979, 1991, 1994, 2002, 2004 (gray shades in Figure 1a). Note, when we apply this methodology to a longer SODA simulation (1901–2008), SODA 2.2.4, we recover the exact partitioning of ENSO events during the time period of overlap from 1958 to 2008 (not shown). Over the full-time period of the SODA 2.2.4 simulation, 16 events are identified as CT El Niños, and 11 as CP El Niño events. This suggests the increase in the frequency of CP El Niños relative to CT El Niños in recent years, which is consistent with the shift in recent decades toward more CP El Niño events (Freund et al., 2019). These events identified in both SODA simulations agree well with the historical HadISST El Niño record from 1900-2008 (Meyers et al., 2007). From now on, we will focus on the analysis of fields from the SODA 2.1.6 (hereafter referred to as SODA).

2.3. Composite Analysis

We have constructed the SODA CT and CP El Niño composites during the year before the El Niño (Year[−1]), the year that leads to the mature phase of El Niño (Year[0] identified in Section 2.2), and the year after the El Niño peak (Year[1]) averaged across the eight CT El Niño and eight CP El Niño events. For the seasonal (3-month average) means, DJF corresponds to December–January–February, MAM corresponds to March-April-May, JJA corresponds to June–July–August, and SON corresponds September-October-November. Statistical significance for the composites is determined using a two-tailed Student's *t*-test, and values significant at 95% confidence and greater are denoted with colored shading.

3. Results

3.1. CT and CP El Nino Composites

To understand the evolution of the TPO associated with CT and CP El Niño events, we carried out a composite analysis on the various surface and subsurface variables. Figure 2 shows the seasonal composites of SST and surface wind stress anomalies, which lead to a mature CT El Niño (Figures 2a–2f) and CP El Niño (Figures 2g–2l) in SODA. An organized evolution of SST and wind stress anomaly patterns are observed over the TPO before the mature phase of the CT El Niño (left panels in Figure 2). During winter of the Year(−1), a surface cooling pattern is present along the equatorial Pacific in response to enhanced easterly trades in this region, consistent with a weak La Niña state (Figures 2a and 2b). In DJF(−1/0), a cyclonic atmospheric circulation is seen over the off-equatorial northwest Pacific, the southern branch of which induces equatorial westerly anomalies in the west Pacific (Figure 2c). By MAM(0), the La Niña type anomalies are replaced by warm SST anomalies in the eastern Pacific, which set up the Bjerknes feedback (Figure 2d). The warm eastern Pacific further strengthens the westerly wind anomalies in the central equatorial Pacific in spring and summer (Figures 2d and 2e) and

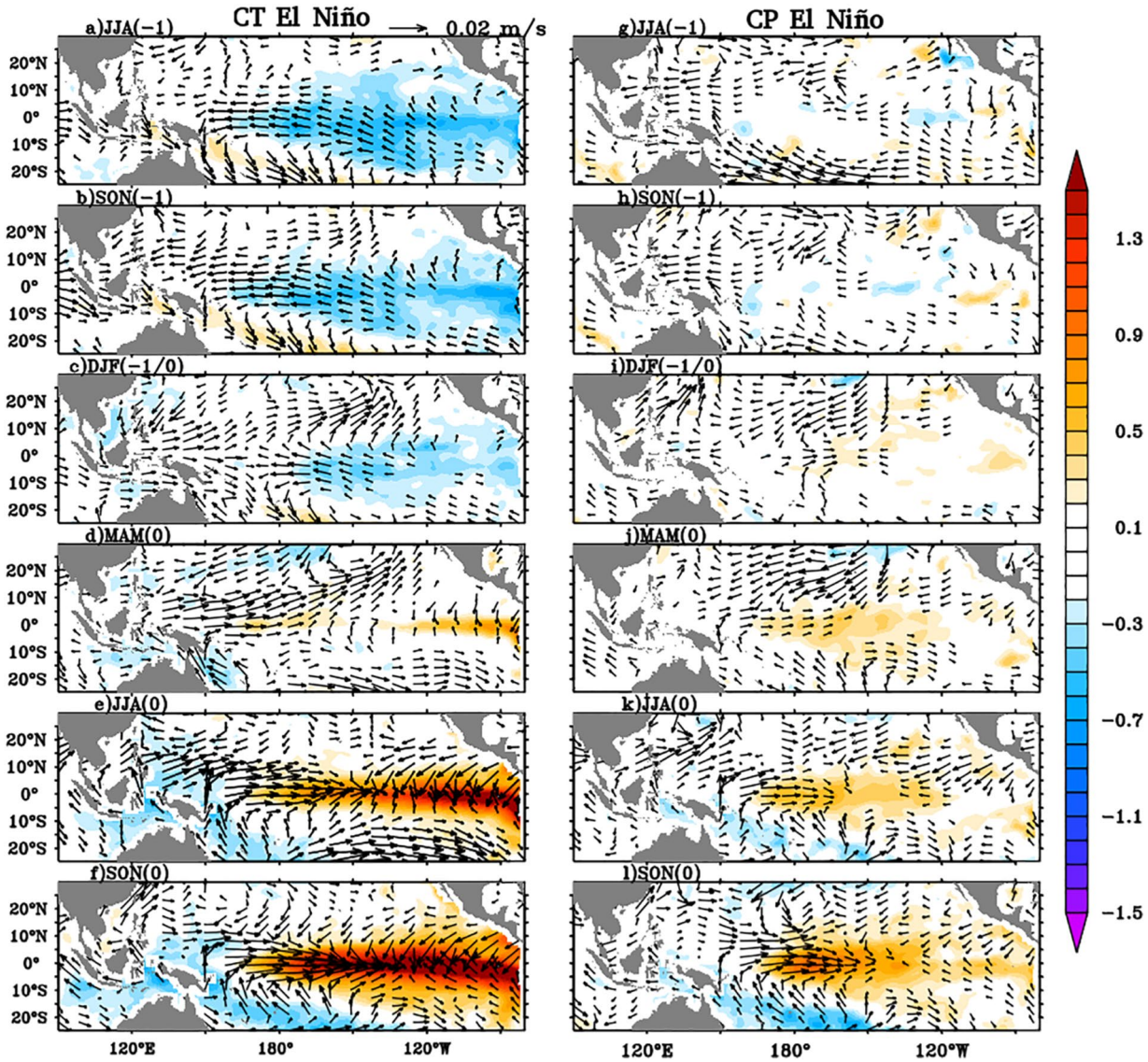

Figure 2. Composite of simple ocean data assimilation (SODA) sea surface temperature (SST) (°C, shaded) and wind stress (Nm^{-2}, vectors) anomalies for (left panels, a–f) Cold Tongue (CT) El Niño and (right panels, g–l) Central Pacific (CP) El Niño events during JJA(−1), SON(−1), DJF(−1/0), MAM(0), JJA(0), and SON(0). Color shading (vectors) show SST (wind stress) values that are significant with 95% confidence. See Section 2.2 for the list of years used for the SODA composites.

enhances the east Pacific warming, which leads to a mature CT El Niño by winter of the Year(0) (Figure 2f). Note that the center of the western Pacific cyclonic circulation pattern shifts eastward during that time.

In contrast, for the CP El Niño, the SST and wind stress anomalies in TPO are not well-organized prior to MAM(0) (Figures 2g–2i), indicating the lack of a robust tropical precursor for CP El Niño events. During MAM(0) (Figure 2j), weak warming commences over the central equatorial Pacific due to the westerly wind stress anomaly in that region. These SST and wind anomalies intensify in the subsequent seasons and lead to a composite CP El Niño (Figures 2k and 2l); however, the anomalies are much less dramatic and localized than for the composite CT El Niño (Figures 2d–2f).

The evolution of subsurface temperature anomalies along the equatorial Pacific (averaged over 3°S–3°N) is shown in Figure 3 for both flavors of El Niño. A year before the mature CT El Niño event, the subsurface warming near the climatological depth of the 20°C isotherm (D20, which serves as a proxy for the mean thermocline depth, red line in Figure 3) reflects the substantial warm water accumulation in the

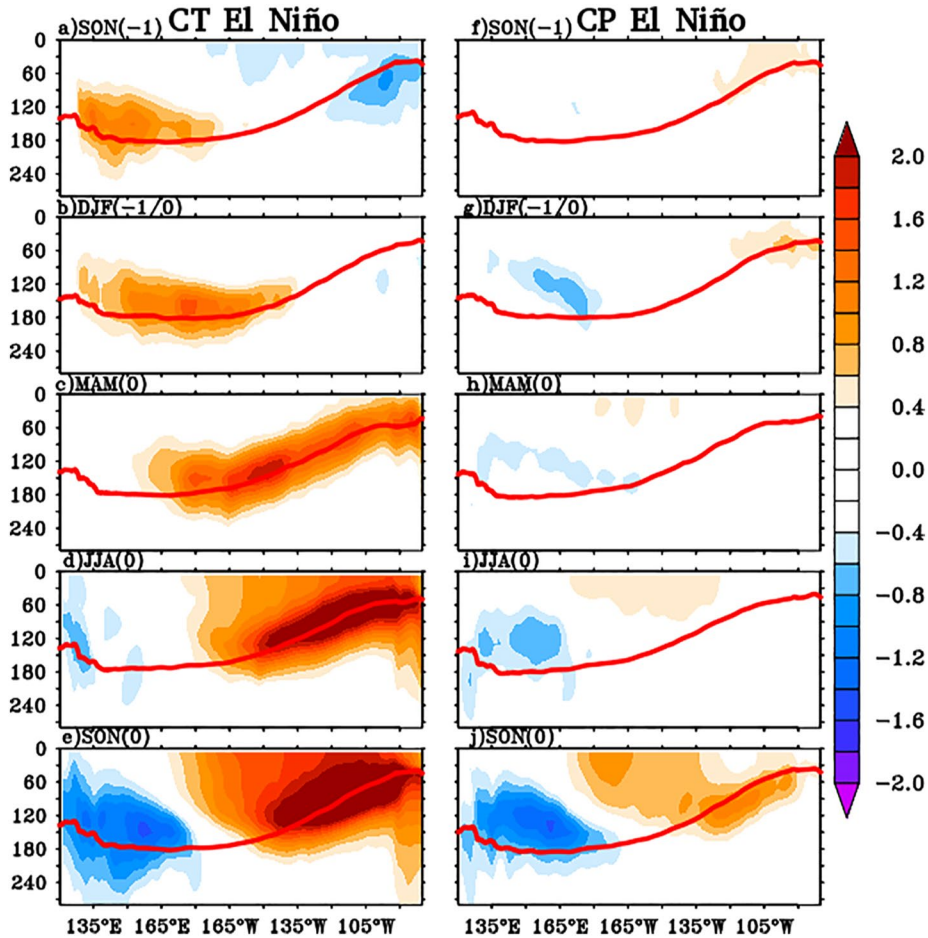

Figure 3. Depth-longitude plots of equatorial Pacific (averaged over 3°S–3°N) subsurface temperature (°C, shaded) anomalies and the depth of climatological 20°C thermocline ([m], red line) for the Simple Ocean Data Assimilation (SODA) (left panels, a–e) Cold Tongue (CT) El Niño and (right panels, f–j) Central Pacific (CP) El Niño composites during SON(−1), DJF(−1/0), MAM(0), JJA(0), and SON(0). Color shading shows the values significant with 95% confidence.

western Pacific (SON[−1], Figure 3a). These warm waters eventually migrate eastward and upward along the zonally tilted thermocline (Figures 3a–3e) and warm the surface layer of the eastern equatorial Pacific in MAM(0). Similar processes are not active, and the warm water accumulation is insignificant during the CP El Niño events (Figures 3f–3j). The central Pacific warming during the CP El Niño becomes apparent in MAM(0) and JJA(0) (Figures 2j, 2k and 3h–3i). This warming is confined in the upper 100 m and is centered near 135°W (Figure 3i). In SON(0), though there is weak warming in the eastern Pacific along the thermocline (Figure 3j), the warming remains mostly confined to the upper layer of the central equatorial Pacific (Figures 2l and 3j). The magnitude of the surface and subsurface warming is significantly weaker in the CP El Niño composite than it is for the CT El Niño composite (compare left and right panels of Figures 2 and 3).

To delve further into the analysis, we also examine the monthly evolution of SODA subsurface heat content (vertically integrated from surface to D20), wind stress, and wind stress curl in Figure 4 from Dec(−1) to Apr(0). In the CT El Niño composite, the presence of two off-equatorial anticyclones (a negative anomaly in NH and a positive anomaly in SH, blue contours in Figure 4a) is evident during Dec(−1). These anticyclonic wind-stress curls, by inducing Ekman downwelling, deepen the thermocline and accumulate the warm water in western TPO. Simultaneously in the far west Pacific, a prominent anomalous cyclonic circulation (positive wind stress curl) appears north of the equator (between 120°E and 140°E and centered at 10°N, Figure 4b), the southern branch of which induces equatorial westerly anomalies in the western Pacific. By Feb(0), this northwest Pacific cyclone shifts eastward and associated equatorial westerly anomalies cross

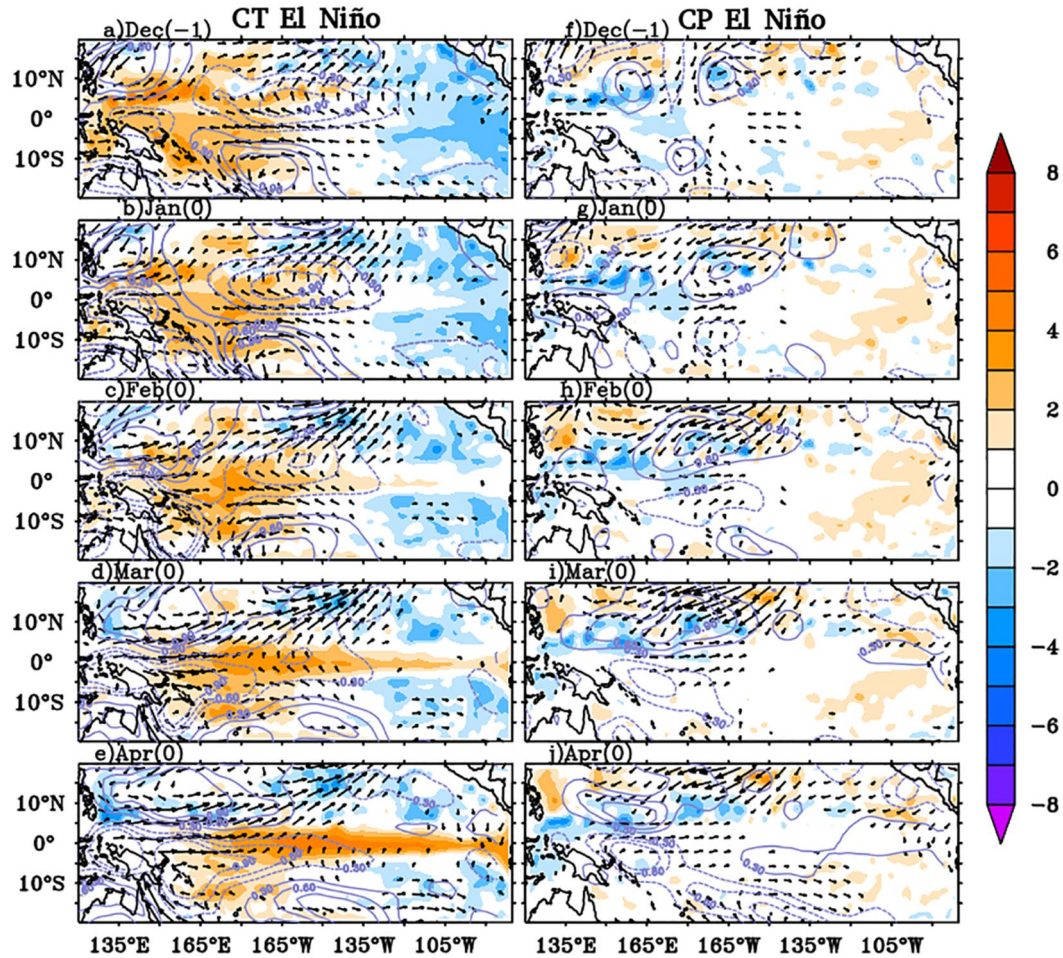

Figure 4. Monthly composite of simple ocean data assimilation (SODA) subsurface heat content (10^9 Jm^{-2}, shaded), wind stress (Nm^{-2}, vectors) and wind stress curl (10^{-8} N m^{-3}, contours) anomalies for (left panels, a–e) Cold Tongue (CT) El Niño and (right panels, f–j) Central Pacific (CP) El Niño during from Dec(−1) to Apr(0). Color shading shows the values significant at 95% confidence.

165°E. These winds push the accumulated warm water eastward and initiate the eastward transport of subsurface warming from the west Pacific along the equatorial waveguide (Figure 4c). In Mar(0)–Apr(0), the entire equatorial thermocline becomes deeper than normal due to the accumulation of warm water over the central and eastern equatorial Pacific (Figures 4d and 4e). The thermocline deepens further in the eastern equatorial Pacific as the surface warming in the eastern Pacific initiates the Bjerknes feedback mechanism (1969). In contrast, the composite of CP El Niño does not exhibit a significant subsurface warming signal in the equatorial Pacific during these five months (Figures 4f–4j).

3.2. ENSO Phase Diagrams

The dependence of Niño3.4 SST anomalies on tropical Pacific upper ocean heat content changes can be further examined using phase diagrams to convey the broader aspects of the cyclic nature and tropical preconditioning of the ENSO cycle. The phase diagram is simply a plot of Niño3.4 SST anomalies versus warm water volume (WWV, the volume of water warmer than 20°C integrated over the region 5°N−5°S, 120°E−80°W) anomalies, which illustrates the lead-lag relationship between the magnitude of WWV changes along the equator and the magnitude of subsequent SST anomalies in the Niño3.4 region. Figure 5 shows the temporal evolution of the composite value of Niño3.4 SST and WWV anomalies in SODA for the CT and CP El Niño from 2 years before the mature phase of El Niño (Year[−2]) to the decaying year of El Niño (Year[1]). During the CT El Niño composite (Figure 5a), the near-circular phase-orbit is consistent

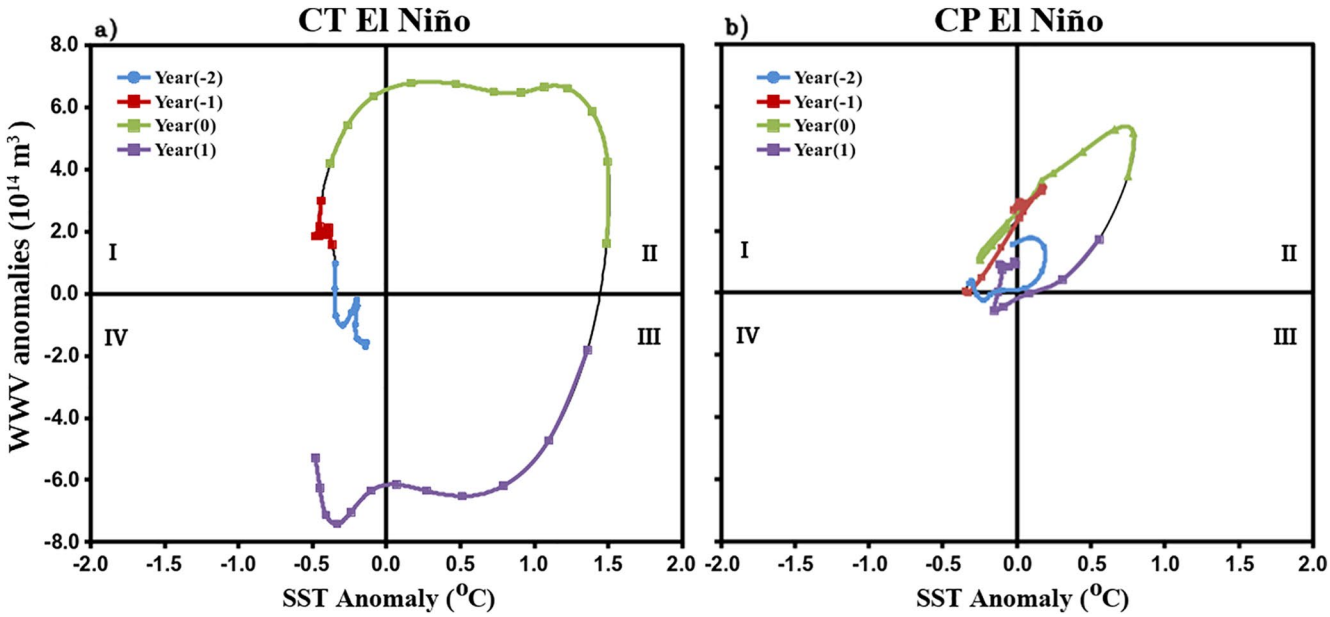

Figure 5. Phase diagrams of the Niño3.4 sea surface temperature (SST) anomalies (°C, along the *x*-axis) and warm water volume (WWV) anomalies (10^{14} m^3) averaged over 5°N–5°S, 120°E–80°W along the *y*-axis for the (a) CT-El Niño and (b) CP El Niño composites in simple ocean data assimilation (SODA). The blue, red, green and purple lines represent the composite evolution during Year(−2), Year(−1), Year(0), and Year(1), respectively. Dots denote each monthly composite value.

with Jin's (1997) recharge-discharge model. It implies that the variation of the Niño3.4 SST is highly correlated with WWV anomalies over the equatorial Pacific, with WWV variability leading the Niño3.4 SST variability by several months. The sequence of this phase diagram is as follows: the first quadrant (with negative SST and positive WWV anomalies) represents the recharge phase, the second quadrant (with positive SST and positive WWV anomalies) represents the El Niño state, the third quadrant (with positive SST and negative WWV anomalies) represents the discharge phase, and the fourth quadrant (with negative SST and negative WWV anomalies) represents the La Niña state (Meinen & McPhaden, 2000). The larger the magnitude of WWV anomalies in the TPO, the stronger the amplitude of SST anomalies in the eastern equatorial Pacific during CT El Niño events. The preponderance of values in the first quadrant of the phase diagram (Figure 5a) suggests the long persistence of near-neutral conditions before a warm El Niño phase. It demonstrates that the initiation of an El Niño event requires a trigger consistent with Figure 2 in Kessler (2002). The relatively smooth phase transition from El Niño to La Niña in Year(1) (positive to negative SSTA in Figure 5a, the purple line moving from quadrant three to quadrant four) is evident for the CT ENSO composite. However, the deviation from a circular shape represents the asymmetry in the ENSO system. In particular, the magnitude of negative SST anomalies (cold) is weaker during the La Niña event than the magnitude of positive SST anomalies (warm) during the preceding CT El Niño event. Note that the phase diagrams for individual CT El Niño events (not shown) behave similarly to the composite.

In contrast, the CP El Niño composite features a quasi-elliptical phase orbit that is mainly confined to the second (positive SST and WWV anomaly) quadrant (Figure 5b) and indicates the rapid adjustment between SST and WWV anomalies over the tropical Pacific during these events. Figure 5b also suggests that the CP El Niños in Year(0) (green line) do not systematically lead to La Niñas in Year(1) (purple line).

We similarly examined the phase diagrams using the Niño3/4 index and found fairly similar orbital motions (not shown). Our phase diagram results confirm that WWV changes in the equatorial Pacific (Cane et al., 1986; Wyrtki 1975, 1985) are helpful predictors of CT Niño events but poor predictors of CP Niño events given the nearly concurrent WWV and SST changes.

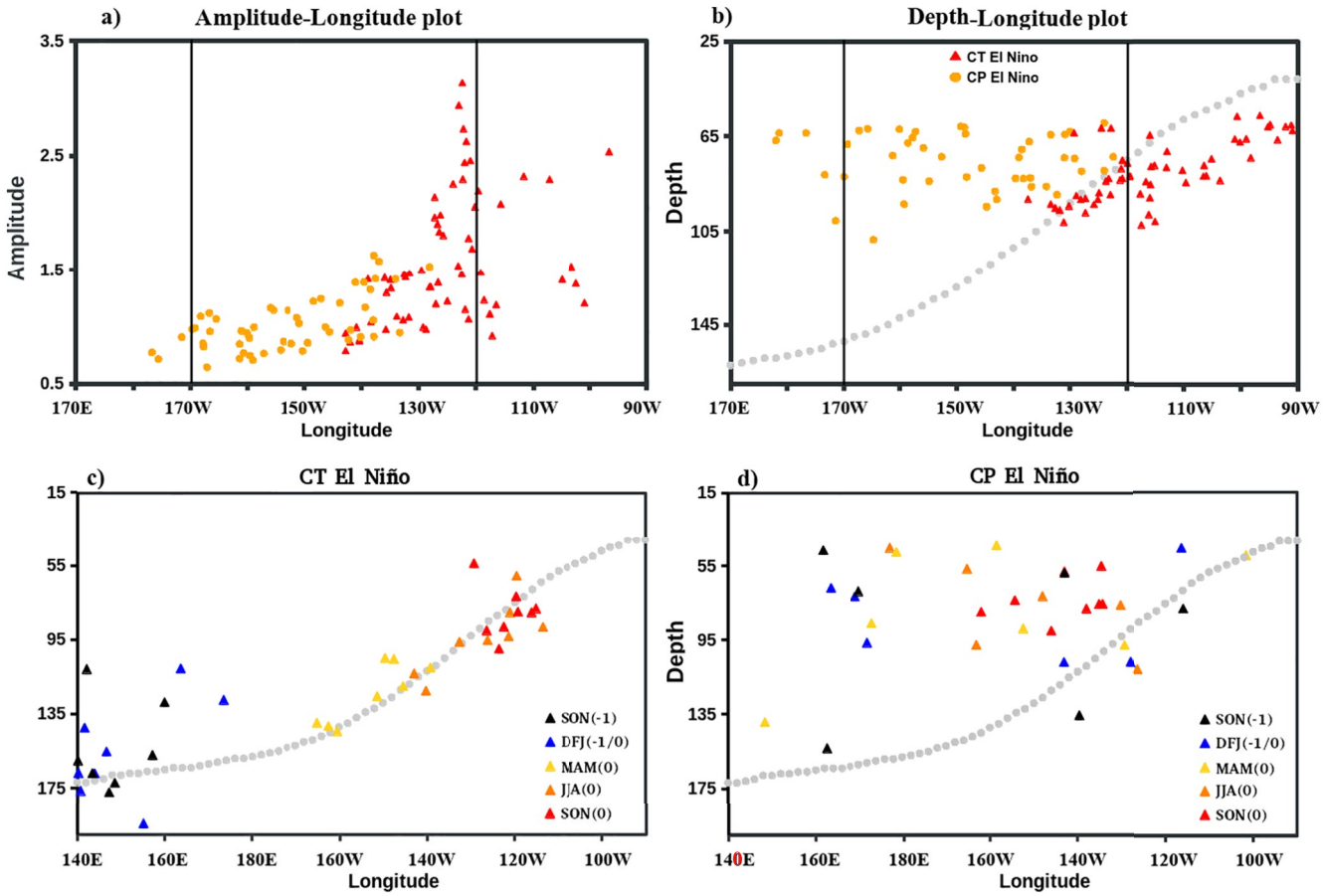

Figure 6. Scatter plots of simple ocean data assimilation (SODA) (a) Surface CHI amplitudes versus longitudes, (b) Sub-CHI depths versus longitudes, red symbols indicate warm months associated with CT El Niño years, and yellow symbols indicate CP El Niño years. Gray symbols are the annual climatological depth of the 20°C isotherm for particular longitude. Scatter plots of the seasonal mean (SON(−1), DJF(−1/0), MAM(0), JJA(0) and SON(0)) sub-CHI depth-longitude plots for individually (c) CT El Niño and (d) CP El Niño events.

3.3. Center of Heat Index (CHI)

The conventional El Niño indices (e.g., Niño3, Niño4, and Niño3.4) are unable to reflect the complex spatial structure of SST and subsurface temperature anomalies during diverse El Niño events because of their fixed areas of interest (zonal limits for Niño3.4 index are shown by black lines in Figures 6a and 6b). By contrast, analysis of the surface CHI (defined in Section 2.2; Giese & Ray, 2011; Ray & Giese, 2012) provides the joint distribution of the longitude and the CHI-amplitude of different El Niño events. We constructed the subsurface CHI (Sub-CHI, Ray & Giese, 2012) to augment the information obtained from the surface CHI index. Sub-CHI is the first moment of equatorial subsurface temperature anomalies (averaged over 2°S–2°N) equal or greater than 1°C and contains information about the depth of maximum warming (Giese & Ray, 2011). We only considered the values of Sub-CHI corresponding to times when the surface CHI is also greater than 0.5°C in an area equal to or greater than the area of the Niño3.4 box. Figure 6a shows the amplitude versus longitude scatter plot of monthly surface CHI for CT El Niño (red triangles) and CP El Niño (yellow dots) events (as defined in Section 2.2). This figure indicates that in SODA, the location of CHIs for CT El Niño events (red triangles) is centered in the eastern Pacific between 140°W and 90°W, with the strongest warming (CHI amplitudes between 1.5°C and 3°C) mainly concentrated east of 130°W. In the case of CP El Niño events (yellow dots), the warming is confined in the longitude range 170°W–130°W (central Pacific), and the amplitude of the warming is considerably weaker (with a maximum amplitude of 1.5°C).

Figure 6b shows the sub-CHI longitude versus sub-CHI depth distribution relative to the climatological mean depth of the thermocline (here D20). This analysis illustrates that the subsurface warming in CT

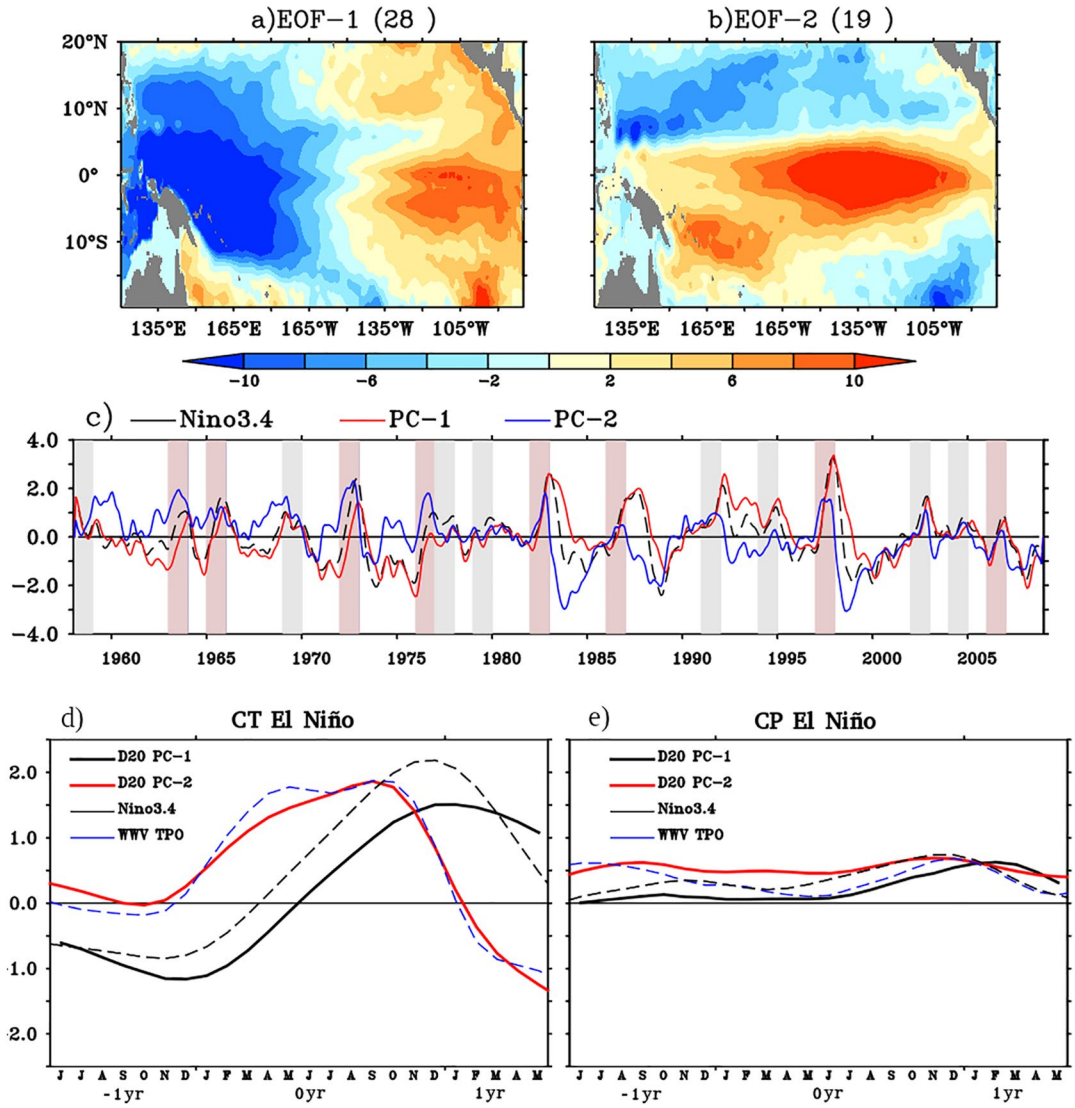

Figure 7. The first two leading EOF modes (a), (b) of simple ocean data assimilation (SODA) D20 (meters) and (c) Their corresponding principal components, PC-1 (red line), PC-2 (blue line) are overlaid onto the Niño3.4 (black dashed line) indices from years 1958 to 2008. The pink and gray vertical bars denote the selected cold tongue (CT) El Niño and Central Pacific (CP) El Niño years, respectively. Temporal evolution of D20 for PC-1 and PC-2, Niño3.4 SST index, and WWV index from Jun Year(−1) to May Year(1) for the (d) CT El Niño and (e) CP El Niño composites.

El Niño events tends to lie close to the mean thermocline (gray dots in Figure 6b). In contrast, subsurface warming in CP El Niño events lies well above the mean thermocline and mainly concentrates in the central equatorial Pacific. Figures 6c and 6d illustrates the temporal evolution of Sub-CHI as a function of depth for the two flavors of El Niño in three-month averages from SON(−1) to SON(0). This figure indicates a coherent eastward propagation and shallowing of Sub-CHI with time during the evolution of the CT El Niños (Figure 6c). However, similar coherent evolution is notably absent during CP El Niños (Figure 6d).

3.4. Leading Modes of Thermocline Variability in the TPO

The dominant patterns of thermocline variability over TPO are identified using EOF analysis applied to the SODA D20 anomalies. Figures 7a and 7b shows the first two leading EOF modes of SODA D20 anomalies in the tropical Pacific and the corresponding principal component (PC) time series (Figure 7c). The first EOF mode reveals an east-west "tilting mode" (Meinen & McPhaden, 2000). It shows a zonal "dipole" pattern of

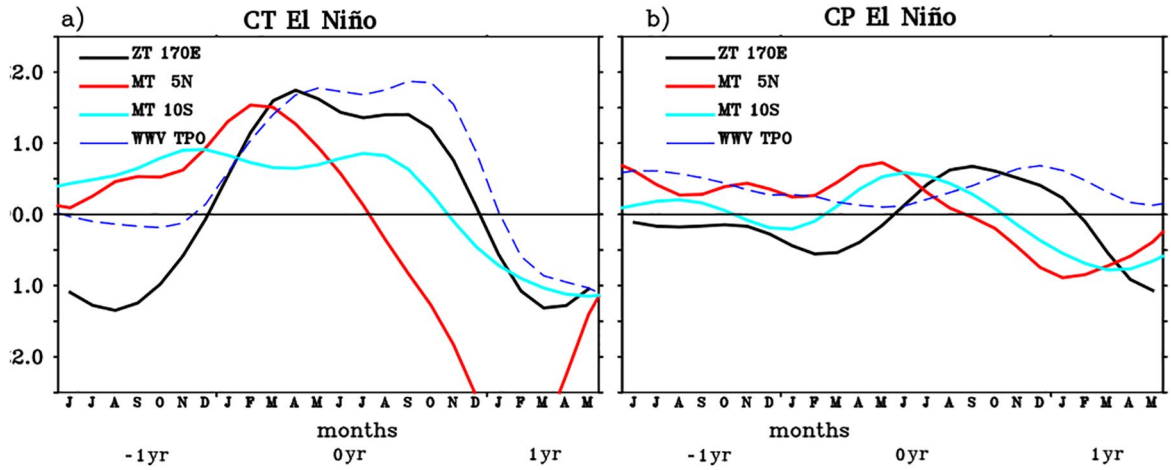

Figure 8. Temporal evolution of normalized (with respect to standard deviation) zonal transport across 170°E (averaged between 10°S and 5°N), meridional transport across 5°N and 10°S (averaged between 140°E and 80°W longitude range), and warm water volume (WWV) index are also compared for (a) Cold tongue (CT) El Niño and (b) Central Pacific El Niño (CP) El Niño composites. Zonal (meridional) transport is defined, so that positive indicates eastward (equatorward) transport.

subsurface heat content which is highly correlated ($r \sim 0.8$, significant at the 95% level) with the Niño3.4. The second EOF mode (Figure 7b) is a "monopole" of positive D20 anomalies (Meinen & McPhaden, 2000). It is highly correlated with WWV anomalies ($r = 0.94$, significant at the 95% level) and represents the recharge phase.

Figures 7d and 7e shows the SODA CT and CP El Niño composites of D20 PC-1, PC-2, along with Niño3.4 SST and WWV anomalies. The changes in WWV over TPO for CT El Niño closely follow the evolution of D20 PC-2 (dash blue and solid red line, respectively, in Figure 7c). The WWV over the TPO begins to increase gradually during the previous winter of CT El Niño. On the other hand, the D20 PC-2, Niño3.4, and WWV evolution during the CP El Niños do not vary significantly, and the anomalies are all substantially weaker (Figure 7e).

3.5. Zonal and Meridional Heat Transports

The Jin (1997) recharge oscillator theory asserts that warm water buildup over the tropical Pacific is driven by the meridional upper ocean heat transport due to wind stress curl. Subsequent studies (Bosc & Delcroix, 2008; Lu et al., 2016; Meinen & McPhaden, 2001), however, have shown that the eastward zonal heat transport also plays a vital role in the buildup of warm water over the central equatorial Pacific (Weisberg & Wang, 1997) during El Niño events. In this section, we intend to examine the influence of zonal and meridional heat transport on the changes in WWV over the equatorial Pacific before and during the CT and CP El Niño events.

Figure 8 shows the normalized zonal heat transport across 170°E and meridional heat transport at 5°N and 10°S (both vertically integrated from the surface to the time-varying 20°C isotherm depth), as well as the normalized WWV anomalies. Figure 8a shows that in the winter prior to CT El Niño events, the accumulation of warm water in the TPO is associated with the equatorward meridional transport of warm water (defined here as positive) across 5°N in the northern hemisphere and 10°S in the southern hemisphere. CT El Niño events start with the rapid buildup in WWV over the equatorial Pacific, which coincides with the eastward zonal transport of warm water at 170°E (Figure 8a, blue dashed and black lines, respectively) in the Years (−1) and (0). During the mature phase of El Niño, the TPO is discharged by the poleward meridional transport (defined here as negative) of the warm water. Note, from Aug(0) onwards, the rapid poleward discharge is evident in the northern hemisphere. However, equatorward meridional transport across 10°S (Figure 8a) suggests that recharge persists for another season in the southern hemisphere. The poleward meridional transport discharges the warm water and finally leads to a La Niña in Year(1).

On the other hand, no sustainable, significant eastward zonal transport (black line in Figure 8b) or equatorward meridional transport (red and cyan lines in Figure 8b) are evident during the year preceding (Year[−1]) the CP El Niño, and the WWV anomalies remain weak throughout this time period (blue dashed line in Figure 8b). During the peak phase of CP El Niño, the westerly wind anomaly over the central Pacific generates very weak equator-ward meridional transport followed by eastward transport along 170°E (Figure 8b), which is not significant. These results support our claim that while the CT El Niño warming is associated with the subsurface recharging and discharging of warm water over the TPO, but that equatorial recharge-discharge cannot explain the CP Cl Niño warming.

4. Summary and Discussion

This study focuses on El Niño diversity concerning the recharge-discharge process and warm water preconditioning using SODA reanalysis data. Past studies (e.g., Cane & Zebiak, 1985; Meinen & McPhaden, 2000; Wyrtki, 1985) have reported the importance of increasing warm water volume in the equatorial Pacific (recharge) as a precursor of El Niño events. The seasonal evolution of surface and subsurface anomalies associated with CT and CP El Niño are shown using the SODA data set. Our analysis reveals that the recharge-discharge process is exclusively related to the CT El Niño events. In contrast, the accumulation of warm water in the TPO prior to CP El Niño is insignificant.

Seasonal composites of CT El Niño evolution show the organized SST and wind anomaly patterns in the TPO before the initiation of the event. Weak La Niña conditions prevail in the preceding year of the CT El Niño (from JJA[−1] to DJF[−1/0]). The stronger than normal easterlies form two off-equatorial anticyclones and via wind-stress curl induced Ekman downwelling accumulate warm water in the west Pacific. In DJF(−1/0), a cyclonic circulation appears in the northwest Pacific, the southern branch of which induces an equatorial westerly in the far western Pacific. In MAM(0), the northwest Pacific cyclonic circulation shifts eastward and the associated equatorial westerly wind stress anomalies pushes the western TPO warm water toward the eastern Pacific. Eventually, it generates the well-known CT El Niño SST signature in subsequent months. In contrast, during CP El Niño events, wind and SST anomaly patterns are not significant until the summer of Year(0). Rather, the CP El Niño warm anomalies appear locally in the upper ocean of the central Pacific in JJA(0), and the anomalies are much weaker and shallower than they are during CT El Niño events.

The surface and subsurface CHI analysis shows distinct separation in the longitudinal position and depth of the peak warming between CT and CP El Niños. The heat content anomalies are deeper and centered further eastward in the CT El Niños than in the CP El Niños. The presence of subsurface warming provides an equatorial thermocline precursor signal for CT El Niño events, and thus it is more predictable with a lead time of approximately one year. The phase orbit diagrams show different relations between eastern Pacific SST and TPO thermocline anomalies for CT and CP El Niño events. The near-circular phase orbits associated with CT El Niño events illustrate the oscillatory behavior of these events. Analysis of zonal and meridional heat transports shows an abrupt increase of WWV during the previous winter of the mature phase of El Niño that is mainly associated with the eastward transport of the warm water from the west to the east Pacific along the equatorial waveguide. On the other hand, the reduction of WWV during and after the mature phase of CT El Niño is driven by poleward transport.

In contrast, for CP El Niño events, the quasi-elliptical phase diagram suggests the rapid adjustment between TPO SST and equatorial thermocline anomalies, thus the absence of a lead-lag correlation between them. The lack of significant warm water buildup prior to these events supports our claim that the tropical subsurface precursor is absent in CP El Niños. This makes the CP El Niño events less predictable in terms of an equatorial thermocline precursor. It is important to note that we do not rule out the predictability of CP El Niños that arises from extratropical Pacific atmospheric forcing, such as through the Pacific meridional mode or trade wind charging mechanism (Anderson et al., 2015; Chakravorty et al., 2021; Pegion et al., 2020; Timmermann et al., 2018). We recognize that extratropical precursors might be the reason for the good prediction skill of CP El Niño events in hindcast simulations (Sun et al., 2018).

In conclusion, this study finds that the recharge/discharge cycle is an integral component or feature of CT El Niño events. The recharge/discharge process does not play any significant role in CP El Niño events.

Data Availability Statement

SODA model fields were obtained from https://www.soda.umd.edu.

Acknowledgments
This work was supported by DST grants (Inspire Faculty Award/2016/DST/INSPIRE/04/2015/000769), India (S. Chakravorty) and NSF grants AGS-1547137 (S. Chakravorty, R. C. Perez) and AGS-1547412 (B. T. Anderson). SC and R. C. Perez acknowledge support from the NOAA/Atlantic Oceanographic and Meteorological Laboratory. S. Chakravorty was supported under the auspices of the Cooperative Institute for Marine and Atmospheric Studies (CIMAS), a Cooperative Institute of the University of Miami and NOAA, cooperative agreement NA20OAR4320472 and IISER, Pune, India. C. Gnanaseelan acknowledges the support of Director, IITM and Ministry of Earth Sciences, Govt. of India. The authors also thank Dr. M. Kersalé and the external reviewers for their helpful comments.

References

Anderson, G., & Perez, R. C. (2015). ENSO and non-ENSO induced charging and discharging of the equatorial Pacific. *Climate Dynamics*, *45*(9–10), 2309–2327. https://doi.org/10.1007/s00382-015-2472-x

Ashok, K., Behera, S. K., Rao, S. A., Weng, H. Y., & Yamagata, T. (2007). El Niño Modoki and its possible teleconnection. *Journal of Geophysical Research*, *112*, C11007. https://doi.org/10.1029/2006jc003798

Bjerknes, J. (1969). Atmospheric teleconnections from the equatorial Pacific[J]. *Monthly Weather Review*, *97*(3), 163–172. https://doi.org/10.1175/1520-0493(1969)097<0163:atftep>2.3.co;2

Bosc, C., & Delcroix, T. (2008). Observed equatorial Rossby waves and ENSO-related warm water volume changes in the equatorial Pacific Ocean. *Journal of Geophysical Research*, *113*, C06003. https://doi.org/10.1029/2007JC004613

Cai, W., Coauthors, S., Lengaigne, M., van Rensch, P., Collins, M., Vecchi, G., et al. (2014). Increasing frequency of extreme ElNiño events due to greenhouse warming. *Nature Climate Change*, *4*, 111–116. https://doi.org/10.1038/nclimate2100

Cane, F., & Zebiak, S. E. (1985). A Theory for El Niño and the Southern Oscillation. *Science*, *228*(4703), 1085–1087. https://doi.org/10.1126/science.228.4703.1085

Cane, M. A., Zebiak, S. E., & Dolan, S. C. (1986). Experimental forecasts of El Niño. *Nature*, *321*, 827–832. https://doi.org/10.1038/321827a0

Capotondi, A., Wittenberg, A. T., Newman, M., Di Lorenzo, E., Yu, J.-Y., Braconnot, P., et al. (2015). Understanding ENSO diversity. *BAMS*, *96*, 921–938. https://doi.org/10.1175/bams-d-13-00117.1

Carton, J. A., & Giese, B. S. (2008). A reanalysis of ocean climate using simple ocean data assimilation (SODA). *Monthly Weather Review*, *136*, 2999–3017. https://doi.org/10.1175/2007mwr1978.1

Chakravorty, S., Chowdary, J. S., & Gnanaseelan, C. (2014). Epochal changes in the seasonal evolution of tropical Indian Ocean warming associated with El Niño. *Climate Dynamics*, *42*, 805–822. https://doi.org/10.1007/s00382-013-1666-3

Chakravorty, S., Perez, R. C., Anderson, B. T., Giese, B. S., Larson, S. M., & Pivotti, V. (2020). Testing the trade wind charging mechanism and its influence on ENSO variability. *Journal of Climate*, *33*(17), 7391–7411. https://doi.org/10.1175/JCLI-D-19-0727.1

Chakravorty, S., Perez, R. C., Anderson, B. T., Larson, S. M., Giese, B. S., & Pivotti, V. (2021). Ocean dynamics are key to extratropical forcing of El Niño. *Journal of Climate*, *34*(21), 8739–8753. https://doi.org/10.1175/JCLI10.1175/jcli-d-20-0933.1

Chattopadhyay, R., Dixit, S. A., & Goswami, B. N. (2019). A Modal Rendition of ENSO Diversity. *Scientific Reports*, *9*, 14014. https://doi.org/10.1038/s41598-019-50409-4

Compo, G. P., Coauthors, J. S., Sardeshmukh, P. D., Matsui, N., Allan, R. J., Yin, X., et al. (2011). The twentieth century reanalysis project. *Quarterly Journal of the Royal Meteorological Society*, *137*, 1–28. https://doi.org/10.1002/qj.776

Fedorov, A. V., Hu, S., Lengaigne, M., & Guilyardi, E. (2015). The impact of westerly wind bursts and ocean initial state on the development, and diversity of El Niño events. *Climate Dynamics*, *44*(5-6), 1381–1401. https://doi.org/10.1007/s00382-014-2126-4

Feng, J., Jin, F., Hu, D., & Guan, S. (2018). Oceanic processes of upper ocean heat content associated with two types of ENSO. *Journal of Oceanography*, *74*, 219–238. https://doi.org/10.1007/s10872-017-0452-y

Feng, J., Wang, L., Chen, W., Fong, S. K., & Leong, K. C. (2010). Different impacts of two types of Pacific Ocean warming on Southeast Asian rainfall during boreal winter. *Journal of Geophysical Research*, *115*, D24122. https://doi.org/10.1029/2010jd014761

Freund, M. B., Henley, B. J., Karoly, D. J., McGregor, H. V., Abram, N. J., & Dommenget, D. (2019). Higher frequency of Central Pacific El Niño events in recent decades relative to past centuries. *Nature Geoscience*, *12*, 450–455. https://doi.org/10.1038/s41561-019-0353-3

Giese, B. S., & Ray, S. (2011). El Niño variability in simple ocean data assimilation (SODA), 1871-2008. *Journal of Geophysical Research*, *116*, C02024. https://doi.org/10.1029/2010JC006695

Ham, Y., & Kug, J. (2012). How well do current climate models simulate two types of El Niño? *Climate Dynamics*, *39*, 383–398. https://doi.org/10.1007/s00382-011-1157-3

Hu, S., & Fedorov, A. V. (2018). Cross-equatorial winds control El Niño diversity and change. *Nature Climate Change*, *8*(9), 798–802. https://doi.org/10.1038/s41558-018-0248-0

Jin, F.-F. (1997). An equatorial ocean recharge paradigm for ENSO. Part I: Conceptual model. *Journal of the Atmospheric Sciences*, *54*, 811–829. https://doi.org/10.1175/1520-0469(1997)054<0811:aeorpf>2.0.co;2

Jin, F.-F., & An, S.-I. (1999). Thermocline and zonal advective feedbacks within the equatorial ocean recharge oscillator model for ENSO. *Geophysical Research Letters*, *26*, 2989–2992. https://doi.org/10.1029/1999GL002297

Johnson, N. C. (2013). How many ENSO flavors can we distinguish? *Journal of Climate*, *26*, 4816–4827. https://doi.org/10.1175/jcli-d-12-00649.1

Kao, H. Y., & Yu, J. Y. (2009). Contrasting eastern-Pacific and central-Pacific types of ENSO. *Journal of Climate*, *22*(3), 615–632. https://doi.org/10.1175/2008jcli2309.1

Karnauskas, K. B. (2013). Can we distinguish canonical El Niño from Modoki? *Geophysical Research Letters*, *4019*, 5246–5251. https://doi.org/10.1002/grl.51007

Karori, M. A., Li, J., & Jin, F.-F. (2013). The asymmetric influence of the two types of El Niño and La Niña on summer rainfall over Southeast China. *Journal of Climate*, *26*, 4567–4582. https://doi.org/10.1175/jcli-d-12-00324.1

Kessler, D. (2002). Is ENSO a cycle or a series of events? *Geophysical Research Letters*, *29*(23), 40-1–40-4. https://doi.org/10.1029/2002GL015924

Kug, J. S., Jin, F. F., & An, S. I. (2009). Two types of El Niño events: Cold tongue El Niño and warm pool El Niño. *Journal of Climate*, *22*, 1499–1515. https://doi.org/10.1175/2008JCLI2624.1

Lee, S. K., DiNezio, P. N., Chung, E. S., Yeh, S. W., Wittenberg, A. T., & Wang, C. (2014). Spring persistence, transition, and resurgence of El Niño. *Geophysical Research Letters*, *41*(23), 8578–8585. https://doi.org/10.1002/2014gl062484

Lee, S.-K., Lopez, H., Chung, E.-S., DiNezio, P., Yeh, S.-W., & Wittenberg, A. T. (2018). On the fragile relationship between El Niño and California rainfall. *Geophysical Research Letters*, *45*, 907–915. https://doi.org/10.1002/2017GL076197

Lee, T., & McPhaden, M. J. (2010). Increasing intensity of El Niño in the central-equatorial Pacific. *Geophysical Research Letters*, *37*, L14603. https://doi.org/10.1029/2010GL044007

Lu, Z., Liu, Z., & Zhu, J. (2016). Abrupt intensification of ENSO forced by deglacial ice-sheet retreat in CCSM3. *Climate Dynamics*, *46*, 1877–1891. https://doi.org/10.1007/s00382-015-2681-3

McPhaden, M. J. (2012). A 21st century shift in the relationship between ENSO SST and warm water volume anomalies. *Geophysical Research Letters*, *39*. https://doi.org/10.1029/2012gl051826

Meinen, C. S., & McPhaden, M. J. (2000). Observations of warm water volume changes in the equatorial Pacific and their relationship to El Niño and La Niña. *Journal of Climate*, *13*, 3551–3559. https://doi.org/10.1175/1520-0442(2000)013<3551:OOWWVC>2.0.CO;2

Meinen, C. S., & McPhaden, M. J. (2001). Warm water displacements in the equatorial Pacific during 1993–1999. *Journal of Physical Oceanography*, *31*, 1324–1345. https://doi.org/10.1175/1520-0485(2001)031<1324:iviwwv>2.0.co;2

Meyers, G., McIntosh, P., Lidia, P., & Mike, P. (2007). The years of El Niño, La Niña, and interactions with the tropical Indian Ocean. *Journal of Climate*, *20*, 2872–2880. https://doi.org/10.1175/jcli4152.1

Newman, M., Shin, S.-I., & Alexander, M. A. (2011). Natural variation in ENSO flavors. *Geophysical Research Letters*, *38*, 14. https://doi.org/10.1029/2011gl047658

Pegion, K., Selman, C. M., Larson, S., Furtado, J. C., & Becker, E. J. (2020). The impact of the extratropics on ENSO diversity and predictability. *Climate Dynamics*, *54*, 4469–4484. https://doi.org/10.1007/s00382-020-05232-3

Picaut, J., Masia, F., & du Penhoat, Y. (1997). An advective–reflective conceptual model for the oscillatory nature of the ENSO. *Science*, *277*, 663–666. https://doi.org/10.1126/science.277.5326.663

Ray, S., & Giese, B. S. (2012). Historical changes in El Niño and La Niña characteristics in an ocean reanalysis. *Journal of Geophysical Research*, *117*, C11007. https://doi.org/10.1029/2012JC008031

Ren, H.-L., & Jin, F.-F. (2011). Niño indices for two types of ENSO. *Geophysical Research Letters*, *38*, L04704. https://doi.org/10.1029/2010GL046031

Ren, H.-L., & Jin, F.-F. (2013). Recharge oscillator mechanisms in two types of ENSO. *Journal of Climate*, *26*(17), 6506–6523. https://doi.org/10.1175/JCLI-D-12-00601.1

Risien, C. M., & Chelton, D. B. (2008). A global climatology of surface wind and wind stress fields from eight years of QuikSCAT Scatterometer data. *Journal of Physical Oceanography*, *38*, 2379–2413. https://doi.org/10.1175/2008jpo3881.1

Singh, A., & Delcroix, T. (2013). Eastern and central Pacific ENSO and their relationships to the recharge/discharge oscillator paradigm. *Deep-Sea Research I*, *82*, 32–43. https://doi.org/10.1016/j.dsr.2013.08.002

Smith, R., Dukowicz, J., & Malone, R. (1992). Parallel ocean general circulation modeling. *Physica D*, *60*, 38–61. https://doi.org/10.1016/0167-2789(92)90225-c

Sun, Q., Bo, W. U., Zhou, T. J., & Yan, Z. X. (2018). ENSO hindcast skill of the IAP-DecPreS near-term climate prediction system: Comparison of full field and anomaly initialization. *Atmospheric and Oceanic Science Letters*, *11*(1), 54–62. https://doi.org/10.1080/16742834.2018.1411753

Takahashi, K., Montecinos, A., Goubanova, K., & Dewitte, B. (2011). ENSO regimes: Reinterpreting the canonical and Modoki El Niño. *Geophysical Research Letters*, *38*, L10704. https://doi.org/10.1029/2011gl047364

Tan, S., & Zhou, H. (2018). The observed impacts of the two types of El Niño on the North Equatorial Countercurrent in the Pacific Ocean. *Geophysical Research Letters*, *45*, 10–493, https://doi.org/10.1029/2018GL079273

Timmermann, A., An, S., Kug, J., Jin, F.-F., Cai, W., Capotondi, A., et al. (2018). El Niño-Southern oscillation complexity. *Nature*, *559*, 535–545. https://doi.org/10.1038/s41586-018-0252-6

Uppala, S. M., Kållberg, P. W., Simmons, A. J., Andrae, U., Costa Bechtold, V. D., Fiorino, M., et al. (2005). The ERA-40 re-analysis. *Quarterly Journal of the Royal Meteorological Society*, *131*, 2961–3012. https://doi.org/10.1256/qj.04.176

Wang, B. (1995). Interdecadal changes in El Niño onset in the last four decades. *Journal of Climate*,*8*, 267–285. https://doi.org/10.1175/1520-0442(1995)008,0267:ICIENO.2.0.CO;2

Wang, C., & Weisberg, R. H. (2000). The 1997–98 El Niño evolution relative to previous El Niño events. *Journal of Climate*, *13*, 488–501. https://doi.org/10.1175/1520-0442(2000)013<0488:tenoer>2.0.co;2

Weisberg, R. H., & Wang, C. (1997). Slow variability in the equatorial west-central Pacific in relation to ENSO. *Journal of Climate*, *10*, 1998–2017. https://doi.org/10.1175/1520-0442(1997)010<1998:svitew>2.0.co;2

Wen, C., Kumar, A., Xue, Y., & McPhaden, M. J. (2014). Changes in tropical Pacific thermocline depth and their relationship to ENSO after 1999. *Journal of Climate*, *27*, 7230–7249. https://doi.org/10.1175/jcli-d-13-00518.1

Wen, N., Li, L., & Luo, J. (2020). Direct impacts of different types of El Niño in developing summer on East Asian precipitation. *Climate Dynamics*, *55*, 1087–1104. https://doi.org/10.1007/s00382-020-05315-1

Wyrtki, K. (1975). El Niño—The dynamic response of the equatorial Pacific Ocean to atmospheric forcing[J]. *Journal of Physical Oceanography*, *5*, 572–584. https://doi.org/10.1175/1520-0485(1975)005<0572:entdro>2.0.co;2

Wyrtki, K. (1985). Water displacements in the Pacific and the genesis of El Niño cycles. *Journal of Geophysical Research*, *90*, 7129–7132. https://doi.org/10.1029/jc090ic04p07129

Xie, R., & Jin, F.-F. (2018). Two leading ENSO modes and El Niño Types in the Zebiak–Cane Model. *Journal of Climate*.

Xu, K., Huang, Q., Tam, C., Wang, W., Chen, S., & Zhu, C. (2019). Roles of tropical SST patterns during two types of ENSO in modulating wintertime rainfall over southern China. *Climate Dynamics*, *52*, 523–538. https://doi.org/10.1007/s00382-018-4170-y

Xu, K., Zhu, C., & He, J. (2013). Two types of El Niño-related Southern oscillation and their different impacts on global land precipitation. *Advances in Atmospheric Sciences*, *30*, 1743–1757. https://doi.org/10.1007/s00376-013-2272-3

Yeh, S., Kug, J., Dewitte, B., Kwon, M.-H., Kirtman, B. P., & Jin, F.-F. (2009). El Niño in a changing climate. *Nature*, *461*, 511–514. https://doi.org/10.1038/nature08316

Yuan, Y., & Yang, S. (2012). Impacts of different types of El Niño on the East Asian climate: Focus on ENSO cycles. *Journal of Climate*, *25*, 7702–7722. https://doi.org/10.1175/jcli-d-11-00576.1